Micromechanical-based criteria for the calibration of cohesive zone parameters

Nawfal Blal [a,b,c], Loïc Daridon [a,c], Yann Monerie [b,c,*], Stéphane Pagano [a,c]

[a] Laboratoire de Mécanique et Génie Civil (LMGC), Université Montpellier 2, CNRS, CC 048 Place Eugène Bataillon, 34095 Montpellier cedex, France
[b] Institut de Radioprotection et de Sûreté Nucléaire, Bat. 702, CE Cadarache, BP3-13115 St. Paul-lez-Durance Cedex, France
[c] Laboratoire de Micromécanique et d'Intégrité des Structures, MIST Laboratory, IRSN-CNRS-Université Montpellier 2, France

ABSTRACT

This paper presents a new micromechanical model for a collection of cohesive zone models embedded between each mesh of a finite element-type discretization. It aims to fully extend the previous linear results of Blal et al. (2012) [11] to the calibration of damageable cohesive parameters (cohesive peak stress, critical opening displacement, cohesive energy, etc). The main idea of the approach consists in replacing the underlying cohesive-volumetric discretization by an equivalent 'matrix-inclusions' composite. The overall behavior of this equivalent composite is estimated using homogenization schemes (Hashin–Shtrikman estimate and the modified secant method) and is given in a closed-form as function of both cohesive and bulk properties and the mesh density. In the particular case of a bilinear cohesive law a micromechanical damage model for quasi-brittle materials is derived. The corresponding local-to-global relationships are obtained for any overall triaxiality loading ratio.

© 2012 Elsevier B.V. All rights reserved.

1. Introduction

Cohesive approaches have emerged as one of the most efficient methods in computational fracture mechanics. However these approaches exhibit strong mesh sensitivity [1,2] and an accurate calibration of the cohesive parameters to extract physically-based macroscopic properties has been until now a cumbersome task [3].

Various (semi-) empirical criteria have been proposed in the last ten years in order to avoid these difficulties (among others, see [4,5]). To fix the idea, a cohesive zone model can be seen as a traction-separation law involving two main parameters: a peak stress R_{max}^{coh} and a cohesive energy G^{coh}. Whatever the shape of the traction-separation law a characteristic length is thus invoked, e.g. G^{coh}/R_{max}^{coh}. The computational challenge is to obtain rigorous criteria linking these characteristic length to the surrounding bulk properties and to the size and the type of the underlying spatial discretization. Previous criteria developed in the literature are mainly limited to unidimensional loadings and no theoretical result is available at any triaxiality loading ratio in three dimensions.

Following a micromechanical-based approach initially proposed by [6], [7] have recently obtained such rigorous criteria for a linear elastic cohesive zone model (no surface damage). We extend here these criteria to any damageable intrinsic cohesive zone model. The main idea is to consider each face of a three dimensional mesh with embedded cohesive zone models as a penny shaped damageable inclusion (Fig. 1). A cohesive-volumetric finite element (CVFE) scheme is thus replaced by a matrix-inclusion composite, and the spatial distribution of inclusions corresponds to the mesh morphology.

* Corresponding author at: Institut de Radioprotection et de Sûreté Nucléaire, Bat. 702, CE Cadarache, BP3-13115 St. Paul-lez-Durance Cedex, France.
E-mail addresses: nawfal.blal@univ-montp2.fr (N. Blal), loic.daridon@univ-montp2.fr (L. Daridon), yann.monerie@irsn.fr (Y. Monerie),
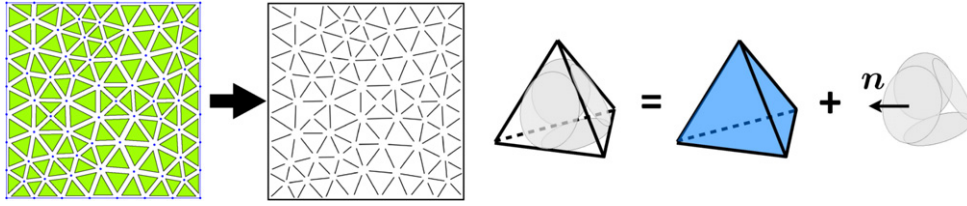stephane.pagano@univ-montp2.fr (S. Pagano).

Fig. 1. Principle of the approach: from a cohesive-volumetric discretization to a 'matrix-inclusions' composite; (left) 2-D illustration, (right) 3-D illustration.

Using a variational approach [8,9] and a linear lower bound [10], a rigorous theoretical estimate of the overall strain potential of this composite is obtained.

Theoretical criteria on cohesive parameters are thus derived from this estimate. The elastic criterion of [7] is recalled (Eq. (21)) and new damageable criteria are proposed. In particular, considering a bilinear cohesive law, closed-form relationships (Eqs. (25)–(30)) between the microscopic cohesive parameters and the macroscopic fracture properties are exhibited through an inverse analysis.

2. Embedding cohesive zone models in bulk media

The proposed micromechanical model is based on a cohesive-volumetric finite element (CVFE) scheme. The overall behavior results in the coupling of the volumetric behavior of bulk elements and the smeared out cohesive surfaces incorporating all softening processes. We focus our attention to elastic bulk behaviors and intrinsic cohesive zone models, i.e. cohesive law with initial stiffness.

2.1. Bulk behavior

We consider the case of linear isotropic elastic media whose behavior is characterized by the constitutive relationships:

$$\boldsymbol{\sigma} = \mathbb{C}^{\mathsf{M}} : \boldsymbol{\varepsilon} \quad \text{with } \mathbb{C}^{\mathsf{M}} = 3k^{\mathsf{M}}\mathbb{J} + 2\mu^{\mathsf{M}}\mathbb{K}, \tag{1}$$

where $\boldsymbol{\sigma}$ (resp. $\boldsymbol{\varepsilon}$) is the stress (resp. strain) field, $\mathbb{C}^{\mathsf{M}}$ is a fourth order stiffness tensor, k^{M} and μ^{M} are the bulk and the shear modulus respectively. The symmetric tensors $\mathbb{J}$ and $\mathbb{K}$ define the generic basis of the fourth order isotropic and symmetric tensors:

$$3\mathbb{J} = \boldsymbol{i} \otimes \boldsymbol{i} \quad \text{and} \quad \mathbb{K} = \mathbb{I} - \mathbb{J} \quad \text{with } 2\mathbb{I}_{ijkl} = (\boldsymbol{i}_{ik}\boldsymbol{i}_{jl} + \boldsymbol{i}_{il}\boldsymbol{i}_{jk}) \tag{2}$$

where $\boldsymbol{i}$ is the second order identity tensor.

2.2. Cohesive zone model

Without loss of generality, any intrinsic cohesive law can be given as a three-dimensional traction-separation law linking the cohesive stress vector $\mathsf{R}^{\mathrm{coh}}$ to the opening displacement vector $[\![\boldsymbol{u}]\!] = \boldsymbol{u}^+ - \boldsymbol{u}^-$, where $\boldsymbol{u}^+$ (resp. $\boldsymbol{u}^-$) is the displacement of the upper (resp. lower) part of the cohesive zone. In a local normal-tangent frame oriented by the normal vector $\boldsymbol{n}$, the opening displacement vector can be decomposed into a normal, u_{N}, and a tangential, $\boldsymbol{u}_{\mathsf{T}}$, component: $[\![\boldsymbol{u}]\!] = u_{\mathsf{N}}\boldsymbol{n} + \boldsymbol{u}_{\mathsf{T}}$. A generic cohesive constitutive relation reads:

$$\mathsf{R}^{\mathrm{coh}} = \boldsymbol{K} \cdot [\![\boldsymbol{u}]\!] \quad \text{with } \boldsymbol{K} = \bar{\beta} \times (C_{\mathsf{N}}\boldsymbol{n} \otimes \boldsymbol{n} + C_{\mathsf{T}}(\boldsymbol{i} - \boldsymbol{n} \otimes \boldsymbol{n})), \tag{3}$$

where C_{N} (resp. C_{T}) is the normal (resp. tangential) initial 'stiffness' of the cohesive law and $\bar{\beta}$ is a surface damage parameter ($\bar{\beta} = 1$ the cohesive zone is undamaged, $0 < \bar{\beta} < 1$ cohesive zone is partially damaged and $\bar{\beta} = 0$ the cohesive zone is fully damaged). Following [2], we assume that the damage parameter $\bar{\beta}$ introduced in (3) depends on the Euclidian norm of the opening displacement vector $[\![\boldsymbol{u}]\!]$, i.e. $\bar{\beta} = \beta(\|[\![\boldsymbol{u}]\!]\|)$ with β a damage function.

3. Micromechanical model

3.1. The cohesive-volumetric finite element scheme as a matrix-inclusion composite

In order to accurately estimate the overall behavior resulting from a CVFE discretization, the procedure proposed in [7] is considered. The idea consists in introducing a continuous *equivalent matrix-inclusion composite* as a convenient representation of the underlying cohesive-volumetric discretization (Fig. 1). The continuous matrix has the same behavior as the bulk finite element behavior (Eq. (1)) whereas the inclusions behavior should represent the cohesive zone model (Eq. (3)). Associating to the inclusions a fictitious thickness e that should tend to zero, and with the help of the strain definition across the cohesive zones:

$$\boldsymbol{\varepsilon}^{\mathrm{coh}} = \frac{1}{2}\frac{[\![\boldsymbol{u}]\!] \otimes \boldsymbol{n} + \boldsymbol{n} \otimes [\![\boldsymbol{u}]\!]}{e}, \tag{4}$$

a damageable fourth order stiffness tensor $\mathbb{C}^{\mathrm{coh}}$ is defined for the cohesive inclusions following [6,7]:

$$\boldsymbol{\sigma}^{\mathrm{coh}} = \mathbb{C}^{\mathrm{coh}}\big(\|[\![\boldsymbol{u}]\!]\|\big) : \boldsymbol{\varepsilon}^{\mathrm{coh}} \quad \text{with } \mathbb{C}^{\mathrm{coh}}\big(\|[\![\boldsymbol{u}]\!]\|\big) = e\beta\big(\|[\![\boldsymbol{u}]\!]\|\big)\Big(C_{\mathrm{N}}\mathbb{E}_l + C_{\mathrm{T}}\mathbb{K}_l\Big) \tag{5}$$

where $\boldsymbol{\sigma}^{\mathrm{coh}}$ is the cohesive stress field and the tensors $\mathbb{E}_l$ and $\mathbb{K}_l$ are two components of the fourth order symmetric and transversely isotropic tensors generic frame:

$$\mathbb{E}_l = \boldsymbol{n} \otimes \boldsymbol{n} \otimes \boldsymbol{n} \otimes \boldsymbol{n}, \qquad \mathbb{K}_l = 2(\boldsymbol{j_s} \otimes \boldsymbol{j_s} + \boldsymbol{j_t} \otimes \boldsymbol{j_t})$$

where $\boldsymbol{j_s} = \boldsymbol{n} \otimes_s \boldsymbol{s}$ and $\boldsymbol{j_t} = \boldsymbol{n} \otimes_s \boldsymbol{t}$ with $\boldsymbol{s}$ and $\boldsymbol{t}$ being two orthogonal vectors defining the transversal plane; $(\boldsymbol{n}, \boldsymbol{t}, \boldsymbol{s})$ define the local orthogonal basis of the cohesive inclusion. We underline that combining (5) and (4), the cohesive stress vector $\mathsf{R}^{\mathrm{coh}} = \boldsymbol{\sigma}^{\mathrm{coh}} \cdot \boldsymbol{n}$ satisfies the constitutive relationship (3).

The cohesive inclusions are distributed according to the spatial distribution of the underlying cohesive-volumetric mesh morphology. Their density, denoted by Z, corresponds to the specific cohesive surface: $Z = \mathcal{A}/\mathcal{S}$ where $\mathcal{A}$ is the total edge length (resp. area) in 2-D (resp. in 3-D) and $\mathcal{S}$ is the total area (resp. volume) of the 2-D (resp. 3-D) meshed body. For a discretization characterized by a mesh size L_{mesh}, $\mathcal{A}$ is proportional to L_{mesh}^{q-1} and $\mathcal{S}$ is proportional to L_{mesh}^{q} where q is the considered dimension. The density Z is thus inversely proportional to the mesh size and can be expressed as:

$$Z = \frac{\gamma}{L_{\mathrm{mesh}}},$$

where the parameter γ depends on the spatial distribution of the considered mesh [11]. In particular, in the case of a statistical isotropic mesh, e.g. a Delaunay-type mesh, the inclusions are randomly distributed in space and in orientation.

Moreover we assume that the cohesive inclusions have a penny-shaped form (Fig. 1). This geometric assumption has no consequence for planar meshes where the edges are replaced by zero thickness whiskers. For 3-D meshes, we suppose that the polygonal edges are replaced by flat disks. We admit that these situations are close to each other but are different in full rigour.

3.2. Overall elastic stiffness

As a first step, the results obtained in [7] for the elastic behaviors are briefly recalled. In this section, the cohesive inclusions behavior is assumed to be linear, i.e. $\bar{\beta} = 1$. The overall behavior of the matrix-inclusion composite is estimated using the Hashin–Shtrikman scheme [10,12] and a lower bound of the overall elastic moduli is derived under the assumption of macroscopic isotropy, i.e. isotropic bulk behavior and isotropic distribution of inclusions (e.g. Delaunay-type meshes). This bound is obtained by considering the inclusions as the reference medium, and the corresponding overall stiffness tensor reads after the passage to limit $e \to 0$ [7]:

$$\mathbb{C}^{\mathrm{hom}} = 3k^{\mathrm{hom}}\mathbb{J} + 2\mu^{\mathrm{hom}}\mathbb{K}, \tag{6}$$

where the overall bulk and shear moduli are respectively given by:

$$\begin{cases} \dfrac{k^{\mathrm{hom}}}{k^{\mathrm{M}}} = \dfrac{\xi^k}{\xi^k + 1} & \text{with } \xi^k = \dfrac{C_{\mathrm{N}}}{Zk^{\mathrm{M}}}, \\[2mm] \dfrac{\mu^{\mathrm{hom}}}{\mu^{\mathrm{M}}} = \dfrac{\xi^\mu}{\xi^\mu + 1} & \text{with } \xi^\mu = \dfrac{15}{4(1 + 3C_{\mathrm{N}}/C_{\mathrm{T}})} \times \dfrac{C_{\mathrm{N}}}{Z\mu^{\mathrm{M}}}. \end{cases} \tag{7}$$

The overall Young's modulus and Poisson ratio associated to this bound read:

$$\frac{E^{\mathrm{hom}}}{E^{\mathrm{M}}} = \frac{\xi^{\mathsf{E}}}{1 + \xi^{\mathsf{E}}} \quad \text{where } \xi^{\mathsf{E}} = \frac{5}{1 + (4/3)(C_{\mathrm{N}}/C_{\mathrm{T}})} \times \frac{C_{\mathrm{N}}}{E^{M}Z}, \tag{8}$$

$$\frac{\nu^{\mathrm{hom}}}{\nu^{\mathrm{M}}} = \frac{15C_{\mathrm{N}}\nu^{\mathrm{M}} + (2C_{\mathrm{N}}/C_{\mathrm{T}} - 1)E^{\mathrm{M}}Z}{15C_{\mathrm{N}}\nu^{\mathrm{M}} + (4C_{\mathrm{N}}/C_{\mathrm{T}} + 3)E^{\mathrm{M}}Z\nu^{\mathrm{M}}}. \tag{9}$$

It is worth noting that Eqs. (7) and (8) show respectively that a cohesive-volumetric formulation with vanishing tangential cohesive stiffness ($C_{\mathrm{T}} \to 0$) leads to a macroscopic no shear ($\mu^{\mathrm{hom}} \to 0$) and no tension ($E^{\mathrm{hom}} \to 0$) material.

3.3. Overall quasi-brittle damage

In this section, the case of non linear damageable cohesive zone models is considered ($0 \leq \bar{\beta} < 1$). The macroscopic stress $\boldsymbol{\Sigma}$ associated to the softening part is obtained via the constitutive law: $\boldsymbol{\Sigma} = \mathbb{C}^{\mathrm{hom}} : \mathsf{E}$, where the homogeneous stiffness tensor $\mathbb{C}^{\mathrm{hom}}$ is estimated using the modified secant method [9], which is equivalent to the Ponte Castañeda variational approach [13]. The non linear stiffness of the inclusions is approached by a secant modulus:

$$\mathbb{C}^{\mathrm{coh}}_{\mathrm{sct}} = \mathbb{C}^{\mathrm{coh}}\left(\sqrt{\big\langle \|[\![\boldsymbol{u}]\!]\|^2 \big\rangle_l}\right), \tag{10}$$

where $\langle . \rangle_I$ denotes the mean value over the cohesive inclusions. This secant stiffness $\mathbb{C}_{sct}^{coh}$ replaces the cohesive tensor $\mathbb{C}^{coh}$ in the Hashin–Shtrikman estimate.

With the help of definition (4), the opening displacement norm $\|[\![u]\!]\|$ can be linked to the fourth order tensor $\mathbb{e} = (1/2)\varepsilon \otimes \varepsilon$ as:

$$\|[\![u]\!]\|^2 = 2e^2(-\mathbb{J} + 2\mathbb{K}) :: \mathbb{e}. \tag{11}$$

Moreover, the generalized Hill lemma allows to derive the second moment of the strain in the inclusion phase $\langle \mathbb{e} \rangle_I$ from the overall elastic energy [14]:

$$\langle \mathbb{e} \rangle_I = \frac{1}{2eZ} \frac{\partial (E : \mathbb{C}^{hom} : E)}{\partial \mathbb{C}_{sct}^{coh}}. \tag{12}$$

Hence, substituting (12) into (11), the mean square root of the opening displacement norm reads:

$$\sqrt{\langle \|[\![u]\!]\|^2 \rangle_I} = \sqrt{\frac{e}{Z}(-\mathbb{J} + 2\mathbb{K}) :: \frac{\partial (E : \mathbb{C}^{hom} : E)}{\partial \mathbb{C}_{sct}^{coh}}}. \tag{13}$$

Involving the hydrostatic part of the strain loading $E_m = (1/3)\mathrm{tr}(E)$ and the equivalent part $E_{eq} = \sqrt{(2/3)E_{dev} : E_{dev}}$ (with E_{dev} being the deviatoric strain tensor: $E_{dev} = E - E_m \boldsymbol{i}$), this last relation is rewritten as:

$$\sqrt{\langle \|[\![u]\!]\|^2 \rangle_I} = \sqrt{AE_m^2 + BE_{eq}^2} \tag{14}$$

where A and B requires to calculate the derivatives $\partial (E : \mathbb{C}^{hom} : E)/\partial \mathbb{C}_{sct}^{coh}$. Due to the specific form of the chosen homogenization scheme, these derivatives can be determined analytically here. In more complicated cases, a numerical derivation can be used as proposed in [15].

Moreover, incorporating an intermediate result of [7] linking the normal-to-tangential cohesive stiffness ratio C_N/C_T to the Poisson ratio:

$$\frac{C_N}{C_T} = \frac{1}{2}\frac{1 + 3\nu^M}{1 - 2\nu^M}, \tag{15}$$

the coefficients A and B are reduced to:

$$A = 2\frac{2 + \nu^M}{1 - 2\nu^M}\left(\frac{3E^M}{E^M Z + 3\bar{\beta}C_N(1 - 2\nu^M)}\right)^2 \tag{16}$$

$$B = \frac{23 + (63 + 82\nu^M)\nu^M}{10(1 + \nu^M)^2}\left(\frac{3E^M}{E^M Z + 3\bar{\beta}C_N(1 - 2\nu^M)}\right)^2. \tag{17}$$

Finally, the expression of the secant modulus is given by:

$$\mathbb{C}_{sct}^{coh} = e \times \bar{\beta} \times (C_N \mathbb{E}_l + C_T \mathbb{K}_l), \quad \text{with } \bar{\beta} = \beta\left(\sqrt{AE_m^2 + BE_{eq}^2}\right). \tag{18}$$

The cohesive secant stiffness tensor $\mathbb{C}_{sct}^{coh}$ is thus obtained solving the non linear problem (18)-right in which A and B depend on the damage parameter $\bar{\beta}$ (see Eqs. (16) and (17)). For any damage function β – i.e. for any shape of the cohesive law – the solution $\bar{\beta}$ of this non linear problem requires generally a numerical method as fixed point schemes. The overall secant behavior is thus derived using the Hashin–Shtrikman bound (6) and (7) and the Eq. (15):

$$\Sigma = \mathbb{C}_{sct}^{hom} : E \quad \text{with } \mathbb{C}_{sct}^{hom} = 3k_{sct}^{hom}(E)\mathbb{J} + 2\mu_{sct}^{hom}(E)\mathbb{K}, \tag{19}$$

where

$$\begin{cases} \dfrac{k_{sct}^{hom}}{k^M} = \dfrac{\xi_{sct}^k}{\xi_{sct}^k + 1} & \text{with } \xi_{sct}^k = \dfrac{\bar{\beta}C_N}{Zk^M}, \\ \dfrac{\mu_{sct}^{hom}}{\mu^M} = \dfrac{\xi_{sct}^\mu}{\xi_{sct}^\mu + 1} & \text{with } \xi_{sct}^\mu = \dfrac{3(1 - 2\nu^M)}{2(1 + \nu^M)} \times \dfrac{\bar{\beta}C_N}{Z\mu^M}. \end{cases} \tag{20}$$

This overall behavior defines a micromechanical damage model whatever the triaxiality loading ratio and the cohesive law type. In Section 4.2, the case of a bilinear cohesive law is discussed: the non linear problem (18)-right can be solved in a closed-form.

4. Inverse identification and practical criteria on cohesive parameters

4.1. Cohesive stiffness

Using cohesive zone models induces an inherent additional compliance that should be controlled. This problem arises naturally for cohesive laws with initial stiffness (intrinsic models) but also for cohesive laws with an initial infinite slope
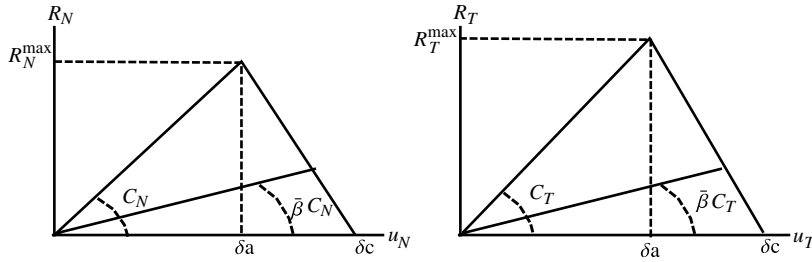
Fig. 2. A bilinear cohesive law: pure opening, $u_T = 0$, (left) and pure shear separation, $u_N = 0$, (right).

(extrinsic models) when dealing with unloading–reloading behaviors. Moreover, the elastic cohesive stiffness is known to be mesh-dependent as illustrated in [1,2].

To overcome these difficulties, some semi-empirical criteria have been proposed in the literature and can be summarized as follows: if L_{mesh} denotes the mesh size of a cohesive-volumetric discretization, the effective elastic stiffness of an elastic medium with embedded cohesive zone model is not significantly disturbed if the condition

$$\frac{C_N L_{\text{mesh}}}{E^M} \geq \alpha$$

is satisfied, where the real α has to be much more larger than 1, e.g. [4,5,2].

Recently, the rigorous micromechanical-based criterion proposed by [11,7]:

$$\frac{C_N L_{\text{mesh}}}{E^M} \geq \gamma \frac{R}{1 - R} \frac{1}{3 - 6\nu^M} \quad \text{and} \quad \frac{C_T}{C_N} = 2 \frac{1 - 2\nu^M}{1 + 3\nu^M} \tag{21}$$

has shown the dependency of α on the bulk Poisson ratio ν^M, on the spatial distribution of the underlying mesh (through γ) and on the apparent stiffness reduction tolerated by the user: $R = E^{\text{hom}}/E^M$.

4.2. Cohesive peak stress and critical opening displacement

Focusing on the case of quasi-brittle elastic materials, we attempt in what follows to derive micromechanical based criteria for the calibration of softening cohesive parameters. For the sake of simplicity, and without any loss of generality, the cases of a bilinear cohesive law (Fig. 2) and of overall pure deviatoric loadings ($\mathbb{J} : E = \mathbf{0}$ and $\mathbb{J} : \Sigma = \mathbf{0}$) are first considered. A procedure is proposed to calibrate the cohesive parameters as a function of: (1) the overall material properties (e.g. experimental data), (2) the shape of the cohesive law, (3) the spatial cohesive-volumetric discretization (mesh morphology and mesh size). These detailed results are then given for the case of overall pure hydrostatic loadings on a crude form.

4.2.1. Overall pure deviatoric loadings

For the case of a bilinear cohesive law, the damage function β reads:

$$\beta \left(\| [\![\boldsymbol{u}]\!] \| \right) = \mathbb{D}_{[0,\delta_a]} \left(\| [\![\boldsymbol{u}]\!] \| \right) + \mathbb{D}_{[\delta_a, \delta_c]} \left(\| [\![\boldsymbol{u}]\!] \| \right) \frac{\delta_a}{\delta_a - \delta_c} \left(1 - \frac{\delta_c}{\| [\![\boldsymbol{u}]\!] \|} \right) \tag{22}$$

where $\mathbb{D}_{[a,b]} (x)$ is the door function equal to 1 if $x \in [a, b]$ and 0 otherwise, δ_a is the opening displacement at the peak cohesive stress for pure normal or tangent loadings, i.e. $R_N^{\text{max}} = C_N \delta_a$ and $\| R_T^{\text{max}} \| = C_T \delta_a$, and δ_c is the critical opening displacement where the complete local failure occurs ($\| R^{\text{coh}} \| = 0$ when $\| [\![\boldsymbol{u}]\!] \| = \delta_c$).

For this bilinear cohesive law, the non linear problem (18) can be solved analytically for the case of pure deviatoric loadings ($E_m = 0$). In particular, an overall damage initiation strain E_{eq}^0 can be defined when the cohesive peak stress is reached:

$$E_{\text{eq}}^0 = \frac{\sqrt{2}(1 + \nu^M)(1 - 2\nu^M)(1 + 3\nu^M)}{\sqrt{\left(1 - 2\nu^M + 5(\nu^M)^2\right) \left(23 + 63\nu^M + 82(\nu^M)^2\right)}} \frac{R_{\text{max}}^{\text{coh}}}{E^M R}, \tag{23}$$

where $R_{\text{max}}^{\text{coh}} = \sqrt{(R_N^{\text{max}})^2 + \| R_T^{\text{max}} \|^2}$ is the maximal cohesive strength. This macroscopic failure initiation depends on the matrix properties E^M and ν^M, on the maximal cohesive strength $R_{\text{max}}^{\text{coh}}$ and on the apparent stiffness reduction R, but does not depend on the morphology γ or the density Z of the mesh. In the same way, the overall critical failure strain E_{eq}^c is reached when the cohesive resistance vanishes ($Z = \gamma/L_{\text{mesh}}$):

$$E_{\text{eq}}^c = \frac{\sqrt{10}(1 + \nu^M)}{3\sqrt{23 + 63\nu^M + 82(\nu^M)^2}} \frac{\gamma \delta_c}{L_{\text{mesh}}}. \tag{24}$$

This critical failure strain does not depend on the Young's modulus of the matrix E^M or on the apparent stiffness reduction R, but increases linearly with respect to the critical opening displacement δ_c and decreases with respect to the mesh size L_{mesh}.

Based on these definitions, three main results can be derived. First, in order to avoid a complete failure occurring before the local surface damage begins, i.e. to satisfy the condition $E^c_{eq} \geq E^0_{eq}$, the critical opening displacement has to respect the condition

$$\delta_c \geq \frac{3}{\sqrt{5}} \frac{(1-2\nu^M)(1+3\nu^M)}{\sqrt{1-2\nu^M+5(\nu^M)^2}} \frac{L_{mesh}}{\gamma R} \frac{R^{coh}_{max}}{E^M}. \tag{25}$$

Hence, we assume in the sequel that the critical opening displacement is linearly proportional to the right part of the inequality (25) through a multiplier coefficient larger than one.

Second, the overall deviatoric strain, $\widehat{E_{eq}}$, leading to the overall deviatoric peak stress $\widehat{\Sigma_{eq}}$, satisfies the equation:

$$\frac{\partial \Sigma_{eq}}{\partial E_{eq}}|_{\widehat{E_{eq}}} = 0 \quad \text{with} \begin{cases} \Sigma_{eq} = \sqrt{(3/2)\boldsymbol{\Sigma} : \mathbb{K} : \boldsymbol{\Sigma}} \\ E_{eq} = \sqrt{(2/3)E : \mathbb{K} : E,} \end{cases} \tag{26}$$

which, once solved, leads to the cohesive-to-overall peak stress relationship:

$$\frac{R^{coh}_{max}}{\widehat{\Sigma_{eq}}} = \frac{\sqrt{2}\sqrt{(1-2\nu^M+5(\nu^M)^2)(23+63\nu^M+82(\nu^M)^2)}}{3(1-2\nu^M)(1+3\nu^M)}. \tag{27}$$

This last ratio can be understood as a stress concentration factor that tends to infinity when the Poisson ratio ν^M of the matrix tends to $1/2$. For practical purposes, this stress concentration factor increases from about 2.7 to 5.4 for ν^M ranging between 0.2 and 0.35. These values have to be compared to 3, corresponding to a circular void in an isotropic and infinite elastic plate subjected to remote loadings. The proposed micromechanical model has thus to be viewed as an effective brittle damage model rather than a model dealing with a single crack propagation.

Third, the overall failure energy $\mathcal{W}_c$ under pure deviatoric loading (the area under the overall stress–strain curve $\Sigma_{eq}-E_{eq}$) is given after integrating (19) from sound material ($\bar{\beta}=1$) to fully damaged material ($\bar{\beta}=0$):

$$\mathcal{W}_c = \int \boldsymbol{\Sigma} : dE.$$

This gives a relationship between the critical opening δ_c and the overall failure energy $\mathcal{W}_c$:

$$\frac{\delta_c}{L_{mesh}} = \frac{3}{\gamma}\sqrt{\frac{2}{5}} \frac{\sqrt{23+63\nu^M+82(\nu^M)^2}}{1+\nu^M} \frac{\mathcal{W}_c}{\widehat{\Sigma_{eq}}}. \tag{28}$$

Based on these three main results and if we are in position to determine, experimentally for example, the macroscopic maximal stress $\widehat{\Sigma_{eq}}$ and the overall energy failure $\mathcal{W}_c$, then the cohesive parameters R^{coh}_{max} and δ_c can be conveniently calibrated as:

$$R^{coh}_{max} = \frac{\sqrt{2}\sqrt{(1-2\nu^M+5(\nu^M)^2)(23+63\nu^M+82(\nu^M)^2)}}{3(1-2\nu^M)(1+3\nu^M)}\widehat{\Sigma_{eq}}, \tag{29}$$

and

$$\delta_c = 3\sqrt{\frac{2}{5}} \frac{\sqrt{23+63\nu^M+82(\nu^M)^2}}{1+\nu^M} \frac{\mathcal{W}_c}{\widehat{\Sigma_{eq}}} \frac{L_{mesh}}{\gamma}. \tag{30}$$

It is clearly shown that the cohesive peak stress depends only on the material Poisson ratio whereas the critical opening is given in terms both of material properties and the mesh quantities L_{mesh} and γ. The criteria resulting from Eqs. (21), (29) and (30) define practical rules to suitably calibrate the cohesive law parameters, namely: (1) the cohesive stiffnesses C_N and C_T, (2) the maximal cohesive stress R^{coh}_{max} and (3) the critical separation δ_c (equivalently the cohesive energy) as functions of the overall material properties (E^M, ν^M) for a given mesh size L_{mesh} and a user-defined elastic reduction $R = E^{hom}/E^M$ (Fig. 3).

Although these results exhibit a mesh dependence of the local cohesive parameters (except R^{coh}_{max} as shown in Fig. 3-left), the proposed approach leads to a *mesh-independent overall behavior* since the macroscopic behavior remains invariant regardless of the mesh size (Fig. 3-right). Indeed, taking into account the previous relationships, the evolution of the macroscopic secant moduli k^{hom}_{sct} and μ^{hom}_{sct} is given as function only of the material properties and the applied macroscopic strain E (cf Eqs. (6), (8) and (21) and here $E_m = 0$):

$$\frac{k^{hom}_{sct}(E)}{k^M} = \frac{\mu^{hom}_{sct}(E)}{\mu^M} = \frac{R\widehat{\Sigma_{eq}}}{\widehat{\Sigma_{eq}}^2 - 6R\mathcal{W}_c\mu^M}\left(\widehat{\Sigma_{eq}} - 2\frac{\mathcal{W}_c}{E_{eq}}\right). \tag{31}$$

Another key point when dealing with cohesive zone models, is the so-called internal cohesive length l^{coh}. Following [16], this characteristic length l^{coh} can be defined as the ratio between the toughness of the material G^{coh} (the area under the
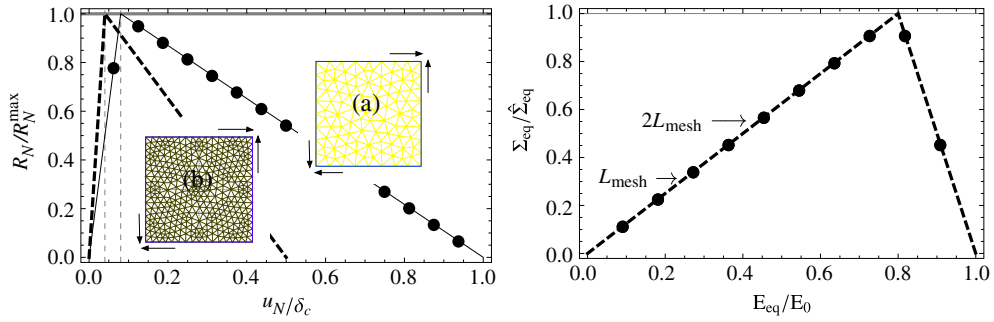
Fig. 3. Cohesive zone model with no mesh sensitivity. Right: the overall material behavior (Eq. (19)) obtained using the bilinear cohesive law (Eq. (22)). Left: The proposed criteria (Eqs. (21)–(30)) for the selection of the cohesive parameters (Table 1): the case of a shear loading for a mesh set of parameters and a user tolerated elastic loss of 5%, i.e. $R = 0.95$ (the material properties are given in Table 1).

Table 1
Mechanical parameters used in Fig. 3. Top: material properties. Bottom: cohesive parameters calibrated using criteria (21), (29) and (30).

E^M (MPa)	ν^M	$\widehat{\Sigma_{eq}}$ (MPa)	$\mathcal{W}_c$ (MPa)
100	1/7	200	100

Mesh	$C_N = C_T$ (GPa)	R_{max}^{coh} (MPa)	δ_c (mm)
(a)	2.6	342.54	1.62
(b)	5.2	342.54	0.81

cohesive stress-opening curve) and the cohesive peak stress, R_{max}^{coh}

$$l^{coh} = \frac{G^{coh}}{R_{max}^{coh}}. \tag{32}$$

It should be noticed that this characteristic length must not be confused with the cohesive length scale over which the cohesive bonds act at the crack tip (process zone), but corresponds to an internal length for the cohesive zone model. For sake of simplicity, defining G^{coh} for mixed modes as:

$$G^{coh} = G_N^{coh} + G_T^{coh} \quad \text{with } G_N^{coh} = \frac{1}{2}C_N\delta_a\delta_c \quad \text{and} \quad G_T^{coh} = \frac{1}{2}C_T\delta_a\delta_c, \tag{33}$$

our approach leads to (see Eqs. (21), (29), (30) and (33)):

$$\frac{l^{coh}}{L_{mesh}} = \frac{3}{5\sqrt{2}\gamma} \frac{3 - \nu^M}{1 + \nu^M} \sqrt{\frac{23 + 63\nu^M + 82(\nu^M)^2}{1 - 2\nu^M + 5(\nu^M)^2}} \frac{\mathcal{W}_c}{\widehat{\Sigma_{eq}}}. \tag{34}$$

It is worth noting that the characteristic cohesive length does not only depend on physical properties, but also on the mesh morphology, on the mesh size and on the loading rate.

4.2.2. Overall pure hydrostatic loadings

For the case of pure hydrostatic loadings ($E_{eq} = 0$), the same procedure gives after some algebra a set of relationships for the calibration of cohesive parameters:

$$R_{max}^{coh} = \frac{\sqrt{10}}{1 + 3\nu^M} \sqrt{\frac{(2 + \nu^M)\left(1 - 2\nu^M + 5(\nu^M)^2\right)}{1 - 2\nu^M}} \widehat{\Sigma_m} \tag{35}$$

and

$$\delta_c = 6\sqrt{2} \sqrt{\frac{2 + \nu^M}{1 - 2\nu^M}} \frac{\mathcal{W}_c}{\widehat{\Sigma_m}} \frac{L_{mesh}}{\gamma}. \tag{36}$$

The combination of (6), (35) and (36) leads to the following equations for the evolution of the macroscopic secant moduli k_{sct}^{hom} and μ_{sct}^{hom} with no mesh-dependency:

$$\frac{k_{sct}^{hom}(E)}{k^M} = \frac{\mu_{sct}^{hom}(E)}{\mu^M} = \frac{R\widehat{\Sigma_m}}{\widehat{\Sigma_m}^2 - 6R\mathcal{W}_c k^M}\left(\widehat{\Sigma_m} - 2\frac{\mathcal{W}_c}{E_m}\right). \tag{37}$$

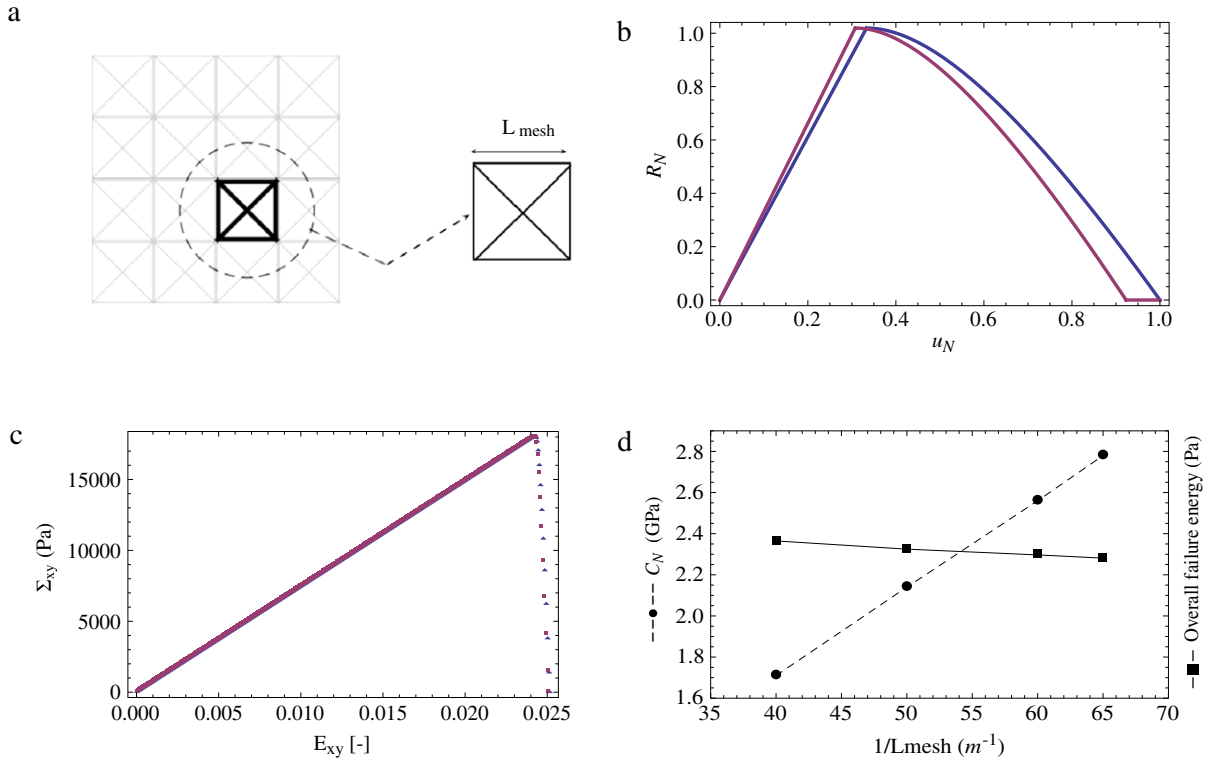This last relationship is similar to the previous one obtained for pure deviatoric loadings (see Eq. (31)).

Fig. 4. Illustration of the mesh-independency of the overall behavior: (a) the unit cell with "crossed-triangle quadrilateral" meshes, (b) the cohesive law (39) calibrated with respect to the obtained micromechanical criteria for two given mesh sizes, (c) the overall deviatoric behavior Σ_{xy} *vs* E_{xy} and (d) the overall mesh-independent failure energy corresponding to the mesh-dependent local cohesive law.

Moreover, using Eqs. (33), (21), (35) and (36), the cohesive length reads:

$$\frac{l^{\text{coh}}}{L_{\text{mesh}}} = \frac{3\sqrt{2}}{\sqrt{5}\gamma}(3 - \nu^{\text{M}})\sqrt{\frac{2 + \nu^{\text{M}}}{(1 - 2\nu^{\text{M}})\left(1 - 2\nu^{\text{M}} + 5(\nu^{\text{M}})^2\right)}}\frac{\mathcal{W}_c}{\widehat{\Sigma_{\text{m}}}}. \tag{38}$$

Again, the same form is obtained as in the deviatoric case (see Eq. (34)) but with a different pre factor depending on the material Poisson ratio. For practical purposes, the cohesive length is about two times larger for pure hydrostatic loadings than for a pure deviatoric one.

5. Numerical validation

The accuracy of the proposed criteria is illustrated in a numerical analysis. In particular, these criteria concern the cohesive parameters but are a priori related to the bilinear shape of the cohesive law. The proposed numerical simulations aim to extend the validity of these criteria to an other shape for the cohesive law. Following [17], a specific form of the cohesive law proposed by [18] is used in this section:

$$\beta\left(\|[\![\boldsymbol{u}]\!]\|\right) = \mathbb{D}_{[0,\delta_a]}\left(\|[\![\boldsymbol{u}]\!]\|\right) + \mathbb{D}_{[\delta_a,\delta_c]}\left(\|[\![\boldsymbol{u}]\!]\|\right)\frac{\delta_c - \|[\![\boldsymbol{u}]\!]\|}{\delta_c/3 + \|[\![\boldsymbol{u}]\!]\|} \tag{39}$$

with

$$\delta_c = 3\sqrt{\frac{w}{9 - 4ln4}\left(\frac{1}{C_{\text{N}}} + \frac{1}{C_{\text{T}}}\right)}$$

where w is a reference surface fracture energy and *ln* the natural logarithm (Fig. 4-(b)).

The simulations concern the case of a unit square cell under a pure shearing loading and considering 2-D plane-strain conditions. The cell is meshed using triangular elements arranged in a "crossed-triangle" quadrilateral pattern (Fig. 4-(a)). The bulk behavior is supposed to be elastic brittle ($E^{\text{M}} = 1$ MPa, $\nu^{\text{M}} = 1/7$, $\widehat{\Sigma_{\text{eq}}} = 6 \times 10^3$ Pa). The software *Xper* [19] is used for the cohesive-volumetric finite element simulations.

As shown in Fig. 4, the numerical results confirm that, even if, the local cohesive parameters are mesh-dependent, the overall fracture properties are mesh-independent: the difference between the critical separation of the cohesive law for the two meshes is about 15%; Fig. 4-(b), while the difference between the critical overall strain and failure energy for the two

meshes is about 0%; Fig. 4-(c) and (d). This mesh-independency is obtained since:

1. the finite element calculus convergence is reached,
2. the cohesive parameters are suitably calibrated for the given mesh type and size.

These results are consistent with previous remarks obtained in the literature (Tijssens et al. [20] for instance).

6. Conclusion

Practical criteria for the calibration of cohesive zone parameters are obtained through a new micromechanical model. This model is based on the study of the overall constitutive behavior of an equivalent 'matrix-inclusions' composite introduced as a representation of a cohesive-volumetric finite element scheme. The approach can be applied whatever the macroscopic triaxiality loading rate and the shape of the cohesive law, extending thus previous partial results from the literature. The case of a bilinear cohesive zone model leads to an overall damage model for quasi-brittle materials. This closed-form model allows to link, through an inverse analysis, all local cohesive parameters to the overall material properties at any given mesh size. The accuracy of the proposed approach and its wide ability to deal with various cohesive laws have been illustrated in a numerical analysis.

References

 [1] S. Song, G. Paulino, W. Buttlar, A bilinear cohesive zone model tailored for fracture of asphalt concrete considering viscoelastic bulk material, Engineering Fracture Mechanics 73 (2006) 2829–2848.
 [2] A. Turon, C. Dãvila, P. Camanho, J. Costa, An engineering solution for mesh size effects in the simulation of delamination using cohesive zone models, Engineering Fracture Mechanics 4 (2007) 1665–1682.
 [3] K. Matouš, M. Kulkarni, P. Geubelle, Multiscale cohesive failure modeling of heterogeneous adhesives, J. Mech. Phys. Solids 56 (2008) 1511–1533.
 [4] H. Espinosa, P. Zavattieri, A grain level model for the study of failure initiation and evolution in polycrystalline brittle materials. part I: theory and numerical implementation, Mechanics of Materials 35 (2003) 333–364.
 [5] V. Tomar, J. Zhai, M. Zhou, Bounds for element size in a variable stiffness cohesive finite element model, International Journal for Numerical Methods in Engineering 61 (2004) 1894–1920.
 [6] V. Acary, Y. Monerie, Nonsmooth fracture dynamics using a cohesive zone approach, Technical Report RR-6032, Institut National de Recherche en Informatique et en Automatique, 2006.
 [7] N. Blal, L. Daridon, Y. Monerie, S. Pagano, Criteria on the artificial compliance inherent to the intrinsic cohesive zone, Comptes Rendus de Mécanique 339 (2011) 789–795.
 [8] P. Ponte Castañeda, The effective mechanical properties of nonlinear isotropic composites, J. Mech. Phys. Solids 39 (1991) 45–71.
 [9] P. Suquet, Overall properties of nonlinear composites: Secant moduli theory and its link with Ponte Castaneda's variational procedure, Comptes Rendus de l'Académie des Sciences 320 (1995) 563–571.
[10] Z. Hashin, S. Shtrikman, A variational approach to the theory of the elastic behaviour of multiphase materials, J. Mech. Phys. Solids 11 (1963) 127–140.
[11] N. Blal, L. Daridon, Y. Monerie, S. Pagano, Artificial compliance inherent to the intrinsic cohesive zone models: criteria and application to planar meshes, International Journal of Fracture (2012) http://dx.doi.org/10.1007/s10704-012-9734-y.
[12] J.R. Willis, Bounds and self-consistent estimates for the overall properties of anisotropic composites, J. Mech. Phys. Solids 25 (1977) 185–202.
[13] P. Ponte Castañeda, P. Suquet, Nonlinear composites, Advances in Applied Mechanics 34 (1998) 171–302.
[14] W. Kreher, Residual stresses and stored elastic energy of composites and polycrystals, J. Mech. Phys. Solids 38 (1990) 115–128.
[15] Y. Monerie, P.-G. Vincent, S. Bourgeois, Overall elastoplastic behavior of anisotropic metal-matrix composites reinforced by aligned inclusions. application to hydrided and irradiated zircaloy-4 cladding tubes, Mechanics of Materials 42 (2010) 175–188.
[16] A. Jaubert, J.-J. Marigo, Justification of Paris-type fatigue laws from cohesive forces model via a variational approach, Continuum Mechanics and Thermodynamics 18 (2006) 23–45.
[17] J.-C. Michel, P. Suquet, An analytical and numerical study of the overall behaviour of metal-matrix composites, Modelling and Simulation in Materials Science and Engineering 2 (1994) 637–658.
[18] F. Perales, S. Bourgeois, A. Chrysochoos, Y. Monerie, Two field multibody method for periodic homogenization in fracture mechanics of nonlinear heterogeneous materials, Engineering Fracture Mechanics 75 (2008) 3378–3398.
[19] F. Perales, F. Dubois, Y. Monerie, B. Piar, L. Stainier, A nonsmooth contact dynamics-based multi-domain solver — code coupling (Xper) and application to fracture, European Journal of Computational Mechanics 19 (2010) 389–417.
[20] M. Tijssens, L. Sluys, E. van der Giessen, Numerical simulation of quasi-brittle fracture using damaging cohesive surfaces, European Journal of Mechanics A/Solids 19 (2000) 761–779.